applied sciences

MDPI

Article

Sorption Behaviour of Ibuprofen Using Activated Carbon Derived from Rose Geranium (*Pelargonium graveolens* L.) Leaves

Patience Mapule Thabede [1,*], Fanyana Mtunzi [2] and Pardon Nyamukamba [3]

[1] Applied Chemistry and Nano Science Laboratory, Department of Chemistry, Vaal University of Technology, P.O. Box X021, Vanderbijlpark 1900, South Africa
[2] Institute of Chemical and Biotechnology (ICBT) Center, Vaal University of Technology, P.O. Box X021, Vanderbiilpark 1900, South Africa
[3] Technology Station Clothing & Textile, Cape Peninsula University of Technology, Symphony Way, P.O. Box 1906, Bellville 7535, South Africa
* Correspondence: mapulepseabelo@gmail.com

Abstract: This research assessed the adsorption of a pharmaceutical compound, ibuprofen, using rose geranium (*Pelargonium graveolens* L.) leaves to prepare low-cost activated carbon through orthophosphoric acid (H_3PO_4) activation. The activated carbon from rose geranium leaves (AC-RGL) was characterized by TGA, SEM and FTIR. The results were compared with those from natural rose geranium leaves (Raw-RGL). The influence of chemical parameters for the uptake of ibuprofen on both adsorbents was evaluated through adsorption experiments. The results were subjected to adsorption models, kinetics models and thermodynamic studies to determine the distribution of ibuprofen in the solid and liquid phases. The results for both Raw-RGL and AC-RGL best fitted the Freundlich model, and the kinetic studies were shown to be pseudo-first order. The thermodynamic evaluation suggested exothermic and spontaneous process sorption for ibuprofen on both adsorbents. The maximum sorption capacities for AC-RGL and Raw-RGL were 113.76 and 74.12 mg/g, respectively. This work confirms that low-cost rose geranium leaves can be used as a potential adsorbent for the sorption of ibuprofen in solution.

Keywords: activated carbon; rose geranium; orthophosphoric; ibuprofen; adsorption

Citation: Thabede, P.M.; Mtunzi, F.; Nyamukamba, P. Sorption Behaviour of Ibuprofen Using Activated Carbon Derived from Rose Geranium (*Pelargonium graveolens* L.) Leaves. *Appl. Sci.* **2023**, *13*, 5133. https://doi.org/10.3390/app13085133

Academic Editor: Francisco José Alguacil

Received: 27 February 2023
Revised: 11 April 2023
Accepted: 17 April 2023
Published: 20 April 2023

1. Introduction

Water contamination is a major environmental concern, and recently, pharmaceutical pollutants in aquatic environments have become a major problem [1,2]. The amount of pharmaceutical products such as ibuprofen (IBP) in the waterways is growing due to human pollution. Ibuprofen is a crystal-like, colorless solid with a distinctive odor [3]. It is the most common non-steroidal anti-inflammatory drug (NSAID) that relieves muscle pain and fever [4]. As with other pharmaceutical products, ibuprofen enters the environment through hospitals, medical effluents and wastewater treatment plants [5,6]. This poses a hazardous impact on the environment due to its bioactive nature. It is becoming ubiquitous in water bodies because conventional water treatment methods cannot effectively remove it.

Due to its everyday existence as a water contaminant and its use in clinical practice, there is a need for its mitigation. The adsorption behavior of ibuprofen onto naturally occurring particulates is hard to characterize due to its complex nature, especially in physicochemical properties and specific functional groups [2]. Different types of adsorbents such as carbon nanotubes [7], plant sludge [8], metal oxides [9,10], microplastics [11], copper particles [12], metal–organic frameworks [13] and activated carbon [14] have been used to adsorb pollutants. Activated carbon (AC) has been proposed as one of the materials for the sorption of ibuprofen from waste water due to its exceptional properties such as porosity, large surface area, high adsorption capacity and diverse functional groups [15]. However, using AC requires expensive precursors and is non-renewable [16]. Thus, using activated carbon with inexpensive and renewable materials has been increasing. Biomass

from *Nigella sativa* L. seeds [17], *Mansonia* [18], cellulose powder [19] and wheat straw [20] have been used to produce activated carbon.

Rose geranium (*Pelargonium graveolens* L.) are large bushy shrubs indigenous to South Africa and found in the Mpumalanga Lowveld, Eastern Cape, Limpopo, Western Cape, Gauteng, North West and KwaZulu-Natal [21–23]. Rose geranium (family Geraniaceae) is also grown in China, Algeria, Morocco, France and Spain [16]. The plant's leaves, flowers and stems contain oil-producing trichomes, producing a pleasant greenish oil dour [24]. Rose geranium is used in the food industry and medical field for its antimicrobial activity [25]. It also has antifungal and antioxidant activity [25]. Rose geranium was selected as the material in this study because it is abundant in nature, easily accessible, inexpensive, eco-friendly, and the plant's surface has functional groups (hydroxyl and carboxyl), making it a good candidate for the adsorption process. The mixture of medicinal and antibacterial properties makes the plant important in water treatment [26]. Hence, this study aimed to evaluate the feasibility of rose geranium for removing ibuprofen from an aqueous medium. Rose geranium was used to assess its nano and pure zeolite capability for remediating lead-polluted soil [27]. No documentation exists on using rose geranium as an adsorbent in water treatment.

Activated carbons (ACs) are materials used as effective sorbents in removing different pollutants [28]. Recently, many researchers have developed new synthesis procedures for ACs from renewable materials such as agro-industrial wastes [29], which have been useful in adsorption studies of organic compounds [30] and toxic metal ions [31]. AC can be made using chemical and physical activation [32]. Physical activation procedures use carbon dioxide and water steam as activating agents, whereas chemical activation methods use chemical reagents [28]. Chemical activation offers better characteristics than physical activation processes, such as lower temperatures, simplicity, lesser activation times, higher yields and development of porous structures of the adsorbents [33]. Potassium hydroxide (KOH) is mostly used to prepare carbons with a high specific surface area with well-developed micropores [34,35]. However, other chemical modifications using phosphoric acid (H_3PO_4) [36,37], sulfuric acid (H_2SO_4) [38], zinc chloride ($ZnCl_2$) [39], hydrochloric acid (HCl) [40] and many others have been used.

The research aimed to prepare a novel low-cost activated carbon from oil-free rose geranium leaves using orthophosphoric acid as a chemical activating agent. The chemically activated material was characterized by scanning electron microscopy (SEM) and Fourier-Transform Infrared (FTIR). The optimum conditions for ibuprofen adsorption were determined for pH, time, temperature and initial concentration. Kinetic and thermodynamic studies were investigated to determine the ibuprofen adsorption process on AC from rose geranium leaves (AC-RGL) and compared with natural rose geranium leaves (Raw-GRL).

2. Materials and Methods

2.1. Materials

Orthophosphoric acid (H_3PO_4) was bought from LabChem (Edenvale, South Africa), and sodium hydroxide (NaOH) and hydrochloric acid (HCl) were bought from Sigma Aldrich (Sigma Aldrich-South Africa, Kempton Park, South Africa). All reagents were of laboratory grade and used without purification. Ibuprofen was purchased from Sigma Aldrich (South Africa).

2.2. Preparation of Activated Carbon

Rose geranium leaves were obtained from the Vaal University of Technology (Sebokeng campus), South Africa. The oil from the leaves was extracted first. After that, the oil-free leaves were pulverized into powder for adsorption experiments. AC was obtained by using the method reported by Thabede et al., 2020 [41]. The pulverized raw leaves were placed in a glass tube, inserted into a furnace with nitrogen, and carbonized at 600 °C, with a heating rate of 10 °C/min for 2 h under nitrogen gas (99.995%). After that, the carbon material was cooled at room temperature under a nitrogen flow. The activation of carbon leaves

was carried out using 0.15 M orthophosphoric acid (H_3PO_4 P) [42]. The carbon material was mixed with 200 mL 0.15 M H_3PO_4 and stirred for 24 h. Subsequently, the mixture was rinsed with ultrapure water several times. The material was dehydrated in an oven at 70 °C overnight. The formed activated carbon was named activated carbon from rose geranium leaves (AC-RGL). The natural rose geranium leaves were called Raw-RGL.

2.3. Adsorption Studies

Experiments were conducted using a 100 mL sample holder with a stopper containing 0.5 g of AC-RGL and 50 mL ibuprofen solution at various concentrations (25, 50, 75, 100 and 120 mg/L). The solutions were mixed in a shaker at 150 rpm for 90 min. The pH was varied at 1, 3, 5, 7 and 9. The contact time was determined for 1, 5, 10, 15, 25, 35, 45, 65, 85 and 105 min, whilst the effect of temperature was assessed at 25, 30, 35, 40, and 45 °C. The above procedure was also used for the Raw-RGL. The pH of the ibuprofen solution was adjusted using 1.0 M NaOH or HCl. The method, as mentioned earlier, was also applied to the Raw-RGL adsorbent. The adequate adsorption stirring speed using Raw-RGL was determined.

2.4. Reusability Tudies

The reusability and regeneration of the Raw-RGL and AC-RGL were accomplished by reusing the IBP-loaded Raw-RGL and AC-RGL adsorbents. The pre-used adsorbents were regenerated by stirring the adsorbents several times in a 0.1 M HNO_3 solution for 15 min to desorb the IBP. Thereafter, the adsorbents were rinsed in distilled water for 30 min.

2.5. Characterization Analysis

Fourier-Transform Infrared (FTIR) spectrometer was used to determine functional groups onto AC-RGL and Raw-RGL before ibuprofen adsorption using a 4000 Nicolet FTIR spectrometer. Images of AC-RGL and Raw-RGL were taken using a Tescan Mira scanning electron microscope (SEM). Thermal gravimetric analyses were conducted using a TGA 4000 thermogravimetric analyzer from Perkin Elmer using nitrogen between 30 and 900 °C. The Brunauer–Emmett–Teller (BET) was used to determine surface area with Micrometrics TriStar II 3020 BET v3.02 with nitrogen as an adsorptive gas. A pH meter from Hach was used for measuring pH of the solution. Remaining Concentration of ibuprofen was conducted on an Evolution 220-UV-Visible spectrophotometer from Thermo Scientific.

3. Results and Discussions

3.1. Thermal Determination

The mass change in AC-RGL and Raw-RGL adsorbents was monitored and recorded between 30 and 900 °C as indicated in Figure 1. The thermogram of the Raw-RGL shows several mass losses up to 850 °C. The first weight loss of approximately 8% due to water loss occurs from 31 °C to 107 °C. The decomposition of hemicellulose, cellulose and lignin accounts for the second weight loss of Raw-RGL of approximately 61% between 107 and 688 °C. The third and final step on Raw-RGL after degradation of lignocellulose material is a tail obtained between 688 and 865 °C due to pyrolysis of the residues. For AC-RGL, the first mass loss of approximately 5% occurs between 31 and 167 °C due to the loss of water molecules, and the second mass loss is in the range of 167–693 °C. In the third step, the weight loss beyond 693 °C indicates the complete decomposition of organic groups. A slight weight loss at 383 and 572 °C observed on Raw-RGL could be due to some bigger unstable molecules [38]. This loss was not observed on AC-RGL.

3.2. Textural Characterization

Figure 2A–D shows the SEM surface morphology of Raw-RGL and AC-RGL. The images indicate that there is a morphological difference between Raw-RGL and AC-RGL. Raw RGL images in Figure 2A,B show an irregular flower-like surface morphology, while SEM images for AC-RGL in Figure 2C,D are made of flat structures with more developed

pores. The carbonization and activation of Raw-RGL were responsible for the porosity development by broadening the pores and creating new ones [43].

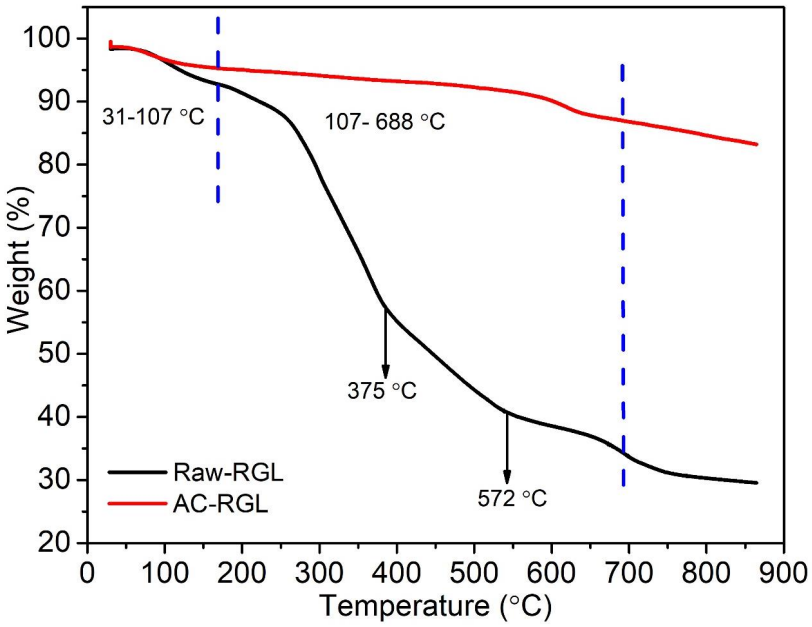

Figure 1. TGA plots of Raw-RGL and AC-RGL adsorbents. The first blue dotted line represent stage 1 which is from the beginning of the graph and end on the blue line, the second stage is the middle of the two blue lines and the third stage is to right after the second blue dotted line.

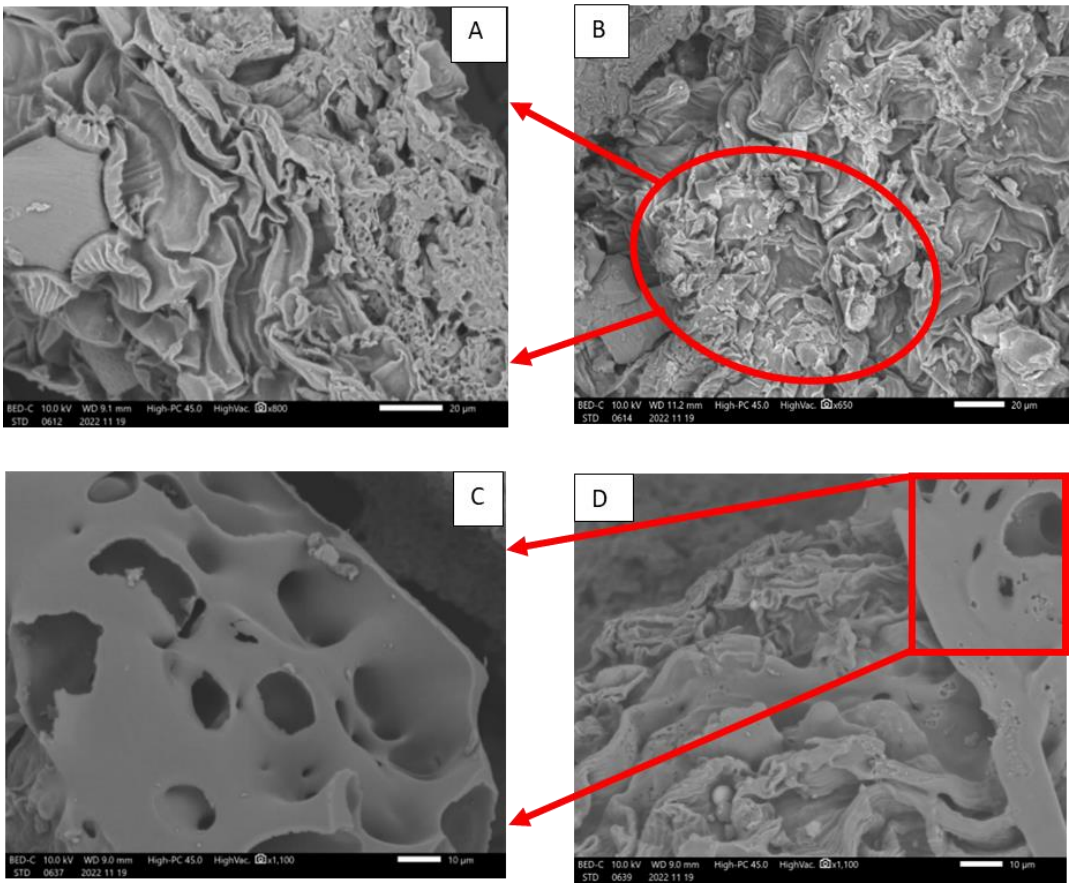

Figure 2. SEM images of Raw-RGL (**A**,**B**) and AC-RGL (**C**,**D**) adsorbents.

3.3. Surface Element Composition

Energy-dispersive X-ray spectroscopy (EDX) is a valuable technique for identifying the elemental composition of the surface of activated carbon [38]. The elemental components regarding mass percentage and the atomic percentage of Raw-RGL and AC-RGL are shown in the EDX spectra of Figure 3A,B. The spectra for both adsorbents show two main components, which are carbon (C) and oxygen (O), which is a characteristic of plant-based materials [44]. Chloride (Cl) is from the coating during sample preparation for SEM analysis. There are other minor peaks corresponding to potassium (K-0.34%) and calcium (Ca-0.37%) on Raw RGL and K (0.56%) and Ca (1.9%) on AC-RGL. Additional peaks for Si (0.64%) and Mg (0.72%) are observed in AC-RGL. The different element ratios are shown in Tables 1 and 2. The higher C and O content is noticed in AC-RGL because of the carbonization and activation of the Raw-RGL. The results produced using EDX agreed with the functional group obtained using (FTIR).

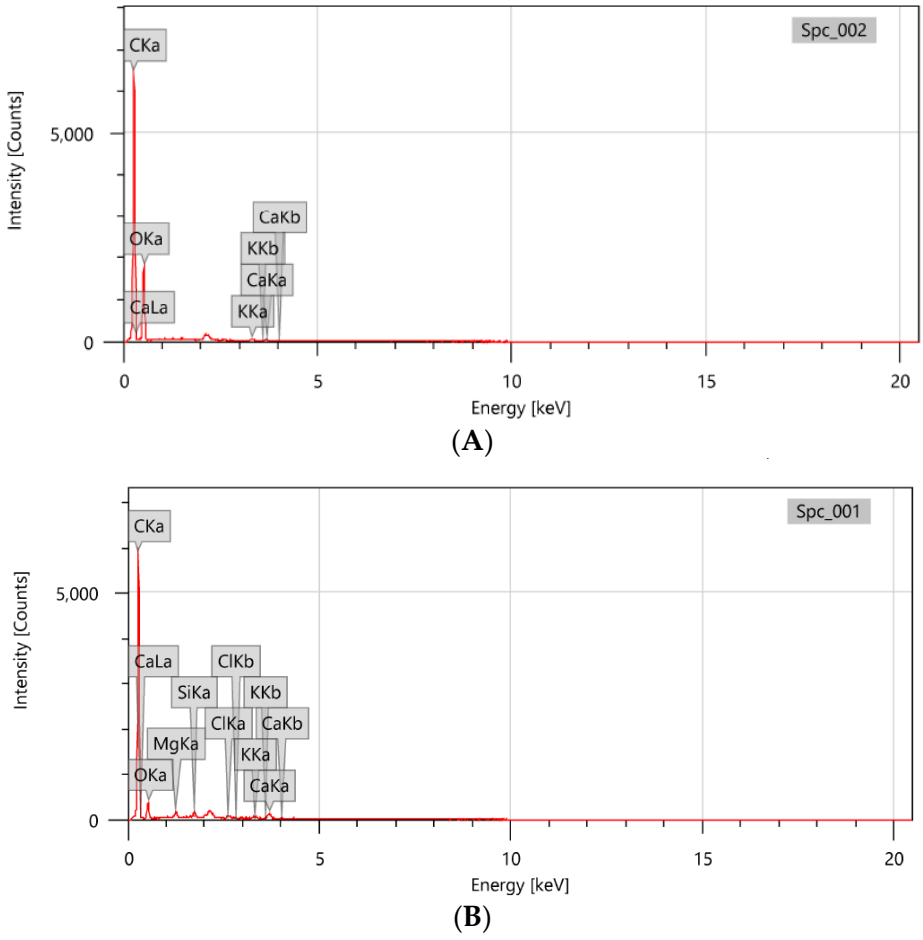

Figure 3. EDX graph of (**A**) Raw-RGL and (**B**) AC-RGL adsorbents.

Table 1. The surface element analysis of Raw-RGL adsorbent.

Element	Mass (%)	Atom (%)
C	62.99	70.12
O	34.90	29.17
K	1.08	0.37
Ca	1.02	0.34
Total	100.00	100.00

Table 2. The surface element analysis of AC-RGL adsorbent.

Element	Mass (%)	Atom (%)
C	77.15	86.05
O	11.46	9.60
Mg	1.30	0.72
Si	1.33	0.64
Cl	1.42	0.54
K	1.63	0.56
Ca	5.70	1.96
Total	100.00	100.00

3.4. Surface Characterization

Infrared spectroscopy is the main instrumental technique used to illustrate the functional groups on AC [45]. The FTIR spectra of Raw-RGL and AC-RGL adsorbents are shown in Figure 4. The spectrum of Raw-RGL shows six major functional groups with a strong, broad vibration at 3287 cm^{-1} due to R-O-H vibrations [46]. The peaks at 2924 and 2842 cm^{-1} are due to aliphatic groups indicated by the vibration of C-H stretching [38]. The absorbance peak between 1731 and 1623 cm^{-1} is attributed to the vibration of carbonyl (-C=O) in the Raw-RGL [47]. The other peak at 1025 cm^{-1} is characteristic of C-OH vibration [48]. A different pattern is observed on AC-RGL whereby the peak at 1558 cm^{-1} is associated with stretching vibrations of -C=O for primary and secondary amides, usually between 1630 and 1520 cm^{-1} [47]. A peak at 1318 cm^{-1} indicates -O-C-O- vibrations [47]. AC-RGL have fewer peaks because most frequencies or functional groups are absent compared with Raw-RGL. The disappearance of the peaks in AC-RGL might be ascribed to the loss of volatile matter at carbonization at 600 °C.

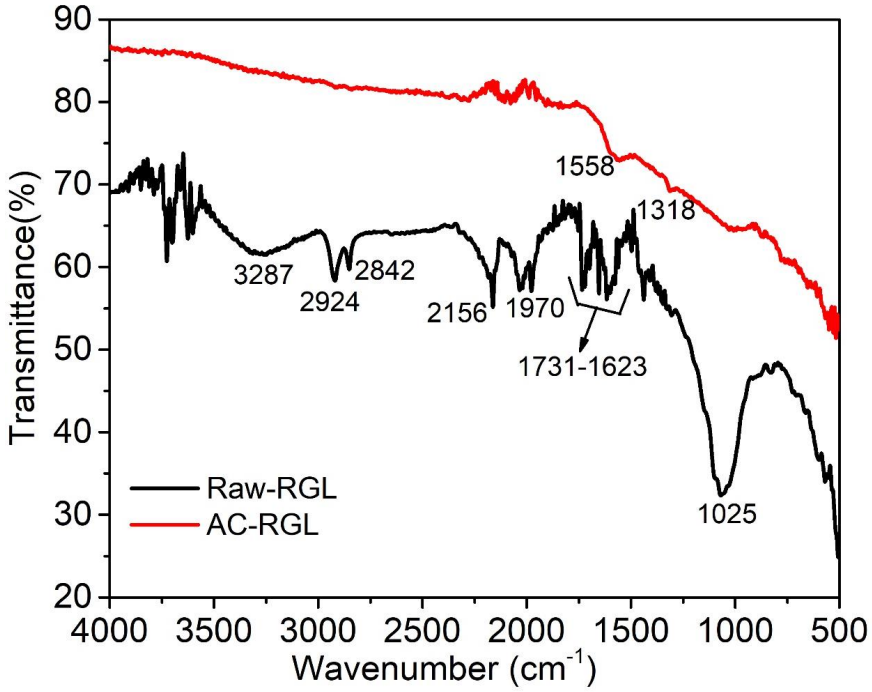

Figure 4. FTIR spectra of Raw-RGL and AC-RGL adsorbents.

3.5. Physicochemical Characterization

The results in Table 3 indicate the data for the physicochemical characterization and zeta potential of the Raw-RGL and AC-RGL. BET results indicated that the surface area of

AC-RGL was 17.69 m^2/g, with a micropore of 0.50 cm^3/g and a mesopore of 0.10 cm^3/g. The total pore of AC-RGL was determined and found to be 0.60 cm^3/g. When comparing the magnitude of the micropore volume with the total pore volume, this contributes approximately 80% of the total pore volume which demonstrate the high microporosity of the AC-RGL. The obtained results proposed that AC-RGL might be the efficient adsorbent in the removal of ibuprofen. The results of $pH_{(PZC)}$ for Raw-RGL and AC-RGL were found to be 7.32 and 6.61, respectively. The results for Raw-RGL were close to neutrality, while those of AC-RGL were slightly acidic. The maximum adsorption of ibuprofen on Raw-RGL was 74.12 mg/g with a zeta potential of 22.56 mV, while AC-RGL capacity was 113.76 mg/g with a zeta potential of 41.13 mV. The AC-RGL with a zeta potential of 41.13 mV adsorbed much more ibuprofen.

Table 3. Physicochemical characterization of Raw-RGL and AC-RGL adsorbents.

Adsorbent	Surface Area (m^2/g)	Micropore Volume (cm^3/gh)	Mesopore Volume (cm^3/g)	Total Pore Volume (cm^3/g)	$pH_{(pzc)}$	Zeta Potential (mV)
Raw-RGL	1.70	-	-	-	7.32	22.56
AC-RGL	17.69	0.500	0.103	0.606	6.61	41.13

3.6. Proposed Adsorption Mechanism of IBP

The proposed adsorption mechanism of IBF onto the adsorbents is shown in Figure 5. Determining the adsorption mechanism(s) is very important. Biodegradation and adsorption are the two ways of removing pharmaceutical compounds which mainly depend on the chemical structure and their operating conditions [49]. Mabungela et al. (2021) [50] also mentioned that functional groups, size and charge of the adsorbent plays a role in determining the adsorption mechanism. There are several mechanisms for the adsorption of ibuprofen on adsorbents such as π–π interactions, hydrophobic, electrostatic hydrogen bonds and cation exchange [49]. Plant materials contain lignocellulosic materials such as cellulose, hemicellulose and lignin [51]. The structure of lignocellulosic materials consists of oxygen-rich functional groups such as (CO), (OH) and (COOH) which might be good candidates for adsorption processes [52]. Additionally, activated carbons developed from lignin materials have revealed promising results for adsorption of different toxic ions including pharmaceutical pollutants [51]. Based on the literature of Singh et al. (2021) [49], the functional groups determined during FTIR analyses in this study suggest that they were involved in the adsorption process, hence the proposed adsorption mechanism in Figure 5.

3.7. Effect of Concentration and Adsorption Models

The concentration effect was determined at 25; 50; 75; 100 and 125 mg/L at a constant temperature (25 °C), and the plots are indicated in Figure 6. The ibuprofen adsorption trend of Raw-RGL and AC-RGL illustrates increased adsorption with increased concentration. The adsorption capacities of Raw-RGL and AC-RGL increase with maxima of 74. 12 and 113.76 mg/g, respectively. The plots show an increased uptake up to 75 mg/L and a decrease after that. The adsorption trend indicates that the AC-RGL had better performance than Raw-RGL. The higher sorption of ibuprofen on AC-RGL could be associated with more active sites being exposed and a higher surface area after the chemical activation of carbon [53].

A comparison of the two models is shown in Table 4 and attained at 298 K (25 °C). Freundlich and Langmuir's isotherms are fitted to estimate the interaction behaviour of ibuprofen onto Raw-RGL and AC-RGL. Table 3 shows that the adsorption data of ibuprofen by Raw-RGL and AC-RGL best fitted the Freundlich model with high regression coefficient (r^2) values of 0.998 and 0.997, respectively. The Freundlich model proposes that the adsorption forms a multilayer adsorbent on the heterogenous surface [46]. A similar observation was made by Sekulic et al. (2019) [54] during the adsorption of IBP.

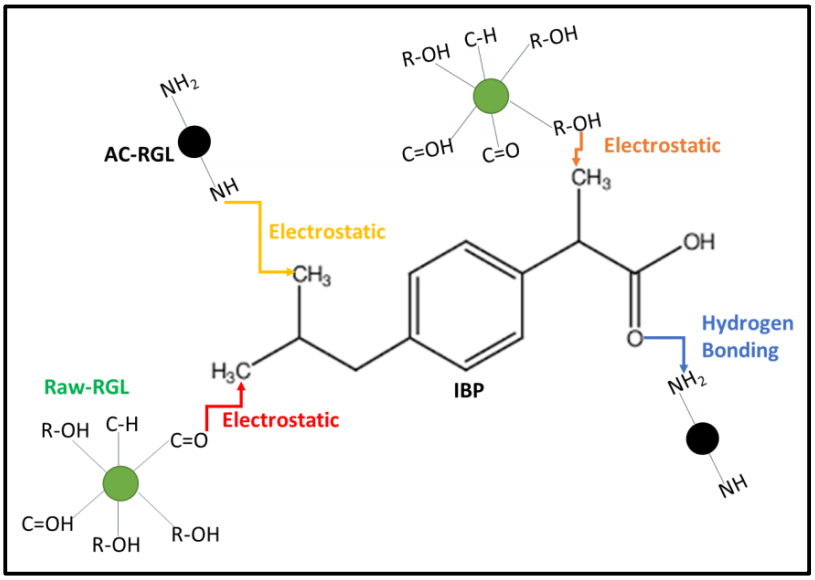

Figure 5. Proposed interaction of Raw-RGL and AC-RGL adsorbents with IBP.

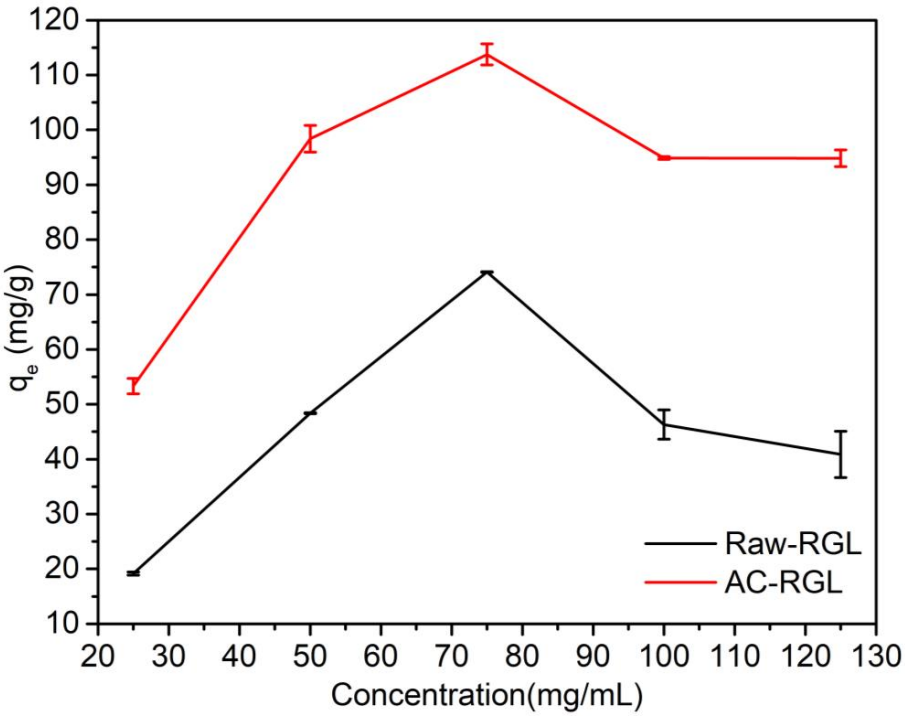

Figure 6. Effect of concentration on ibuprofen uptake by Raw-RGL and AC-RGL adsorbents.

Table 4. Adsorption isotherms of Raw-RGL and AC-RGL and parameters.

Isotherms		Raw-RGL	AC-RGL
Langmuir	Q_o	45.12	35.68
	B	2.13	3.82
	r^2	0.812	0.951
Freundlich	1/n	69.67	125.68
	k_f	3.67	1.67
	r^2	0.998	0.997
Experimental (q_e)		74.12	113.76

3.8. Time Effect and Rate Kinetics

The results of ibuprofen adsorption by Raw-RGL and AC-RGL are indicated in Figure 7 and show that the uptake of ibuprofen is fast at the beginning of the adsorption process. The rapid uptake of ibuprofen is due to various active sites. The uptake of ibuprofen was particularly fast within the initial 1–35 min interval by the Raw RGL. From 45 to 105 min, the sorption slowly decreased due to sites being filled and therefore restricted [55]. The reaction rate onto AC-RGL was quicker and occurred between 1 and 10 min compared with the Raw-RGL. The maximum sorption capacities were 68.97 and 101.96 mg/g for the Raw-RGL and AC-RGL.

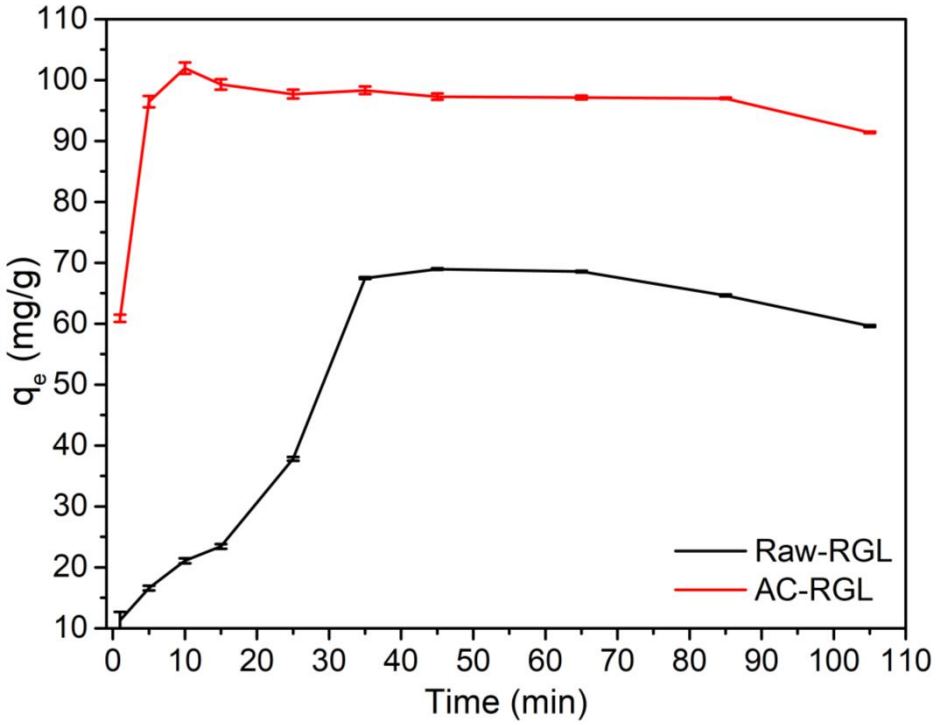

Figure 7. Effect of time on ibuprofen uptake by Raw-RGL and AC-RGL adsorbents.

The kinetic data of ibuprofen adsorption by Raw-RGL and AC-RGL were fitted into the pseudo-first-order (PFO), pseudo-second-order (PSO) models and intraparticle diffusion (IPD) and the data are shown in Table 5. This was done to estimate whether the adsorption process fit the PFO, PSO, or IPD models. The best-fit model must have a correlation coefficient close to 1. Table 4 shows that PFO was the best fit with r^2 of 0.995 and 0.993 for Raw-RGL and AC-RGL, respectively. The best fit for PFO shows that the uptake of ibuprofen by Raw-RGL and AC-RGL involves Van der Waal forces of attraction and that process was physisorption [56]. IPD kinetic estimation shows whether adsorption occurred in the pores or the surface. Table 4 shows that the estimated surface adsorption (ESA) was the main process compared with the estimated pore adsorption (EPA). ESA is between 83.12 and 87.12%, and EPA ranges from 12.88 to 16.88%.

3.9. Temperature and Thermodynamic Parameters

The temperature parameters for Raw-RGL and AC-RGL were evaluated at five temperatures: 25 °C (298 K), 30 °C (308 K), 35 °C (318 K), 40 °C (328 K), and 45 °C (338 K); and the experimental data are shown in Figure 8. The adsorption trends for Raw-RGL and AC-RGL are similar, showing a rise in sorption capacity with a temperature increase from 25 to 35 °C. Later, less adsorption capacity was observed when the temperature increased between 40 and 45°C. That implies that only a slight energy increase was required for adsorption. The maximum sorption capacities for Raw-RGL and AC-RGL adsorbents are 64.03 and 104.74 mg/g at 35 °C, respectively.

Table 5. Kinetic studies of Raw-RGL and AC-RGL and their parameters.

Models		Raw-RGL	AC-RGL
PFO	K_1	0.469	0.979
	r^2	0.995	0.993
PSO	q_e	34.56	56.65
	K_2	0.101	1.002
	r^2	0.861	0.757
IPD	C	33.23	47.23
	K_i	7.715	13.06
	r^2	0.867	0.823
EPA	%	12.88	16.88
ESA	%	87.12	83.12
Experimental (q_e)		68.97	101.96

EPA—estimated pore adsorption of IPD; ESA—estimated surface adsorption of IPD.

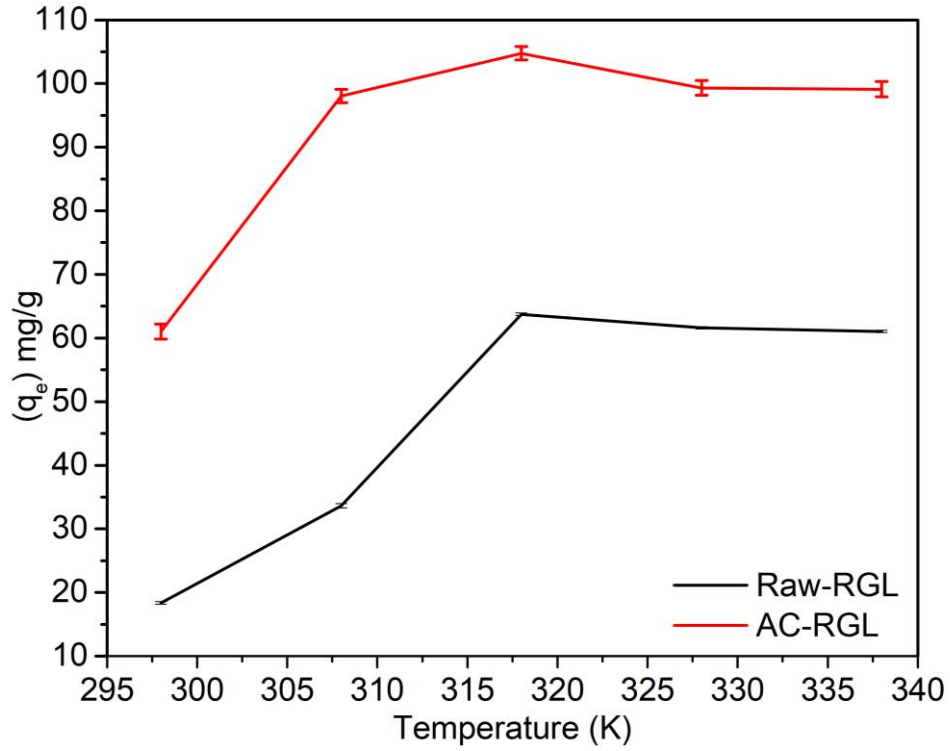

Figure 8. Effect of temperature on ibuprofen uptake by Raw-RGL and AC-RGL adsorbents.

Thermodynamic parameters are vital for investigating heat variation and the spontaneity of the sorption process [57]. ΔG°, ΔH°, and ΔS° are calculated at different temperatures (298; 308; 318; 328 and 338 K) of ibuprofen on Raw RGL and AC-RGL sorbents and indicated in Table 6. The ΔH° results for both adsorbents indicate that the sorption processes are exothermic. The size of ΔH° of ibuprofen adsorption suggests a weak interactive strength, which also suggests electrostatic attraction [55]. ΔS° data for ibuprofen adsorption by Raw-RGL and AC-RGL indicate an increase in the randomness of ibuprofen in solution as the adsorption reaches equilibrium. The ΔG° figures for both adsorbents indicate that the uptake process is spontaneous and feasible.

Table 6. Thermodynamic studies of Raw-RGL and AC-RGL and their parameters.

Parameter	Raw-RGL	AC-RCL
ΔH° (KJ mol^{-1})	−2.39	−2.34
ΔS° (KJ $mol^{-1}K^{-1}$)	3.23	4.78
ΔG° (KJ mol^{-1}) 298 K	−4.67	−3.80
308 K	−5.65	−4.89
318 K	−6.45	−5.23
328 K	−7.55	−6.01
338 K	−8.43	−6.89

3.10. pH Effect

The cations of the solution pH are very important because they influence the charge of the sorption process, thus affecting the process's extent [58]. Figure 9 shows the effect of pH ranging from 1 to 9 for both adsorbents. The removal capacity of ibuprofen increases as the pH increases from 1 to 5 on both adsorbents, with a maximum capacity observed at pH 5. The adsorption due pH increases were due to the lower electrostatic repulsion between ibuprofen and the activated carbon surface. With a pH greater than 7, the uptake for ibuprofen decreased. Less ibuprofen uptake in neutral to basic condition might due to be competition between protons and ibuprofen for site availability [36].

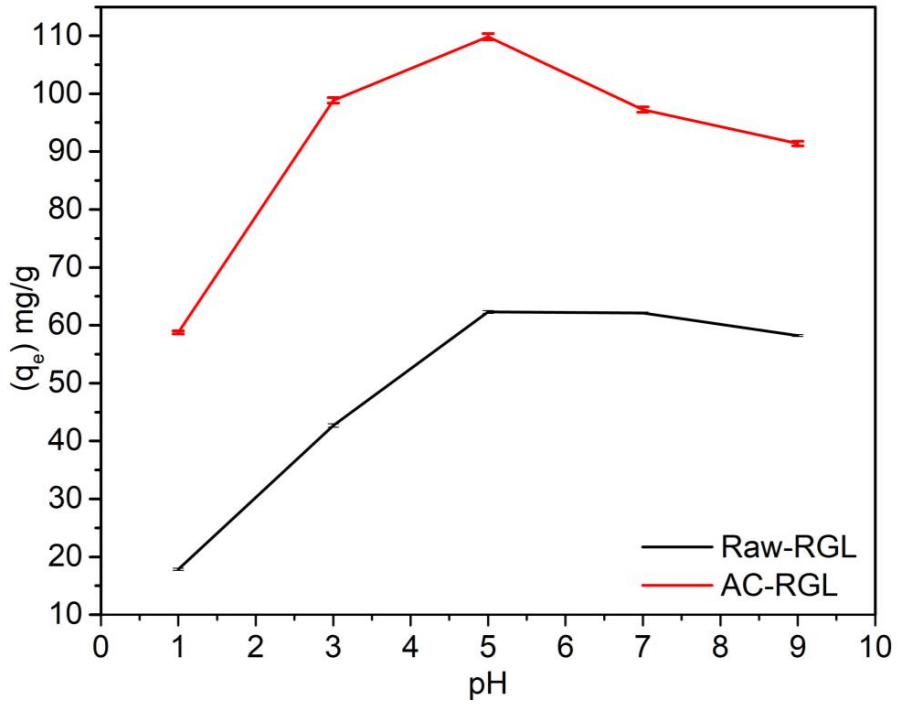

Figure 9. Effect of pH on ibuprofen uptake by Raw-RGL and AC-RGL adsorbents.

3.11. Stirring Speed Effect

The stirring speed is a vital factor influencing the adsorption rate [59]. The stirring speed effect was studied using 50 mL of solution for 90 min at 25 °C, and different stirring speeds ranging from 50 to 250 rpm. The adsorption capacity versus different stirring rates is shown in Figure 10. The data showed that the adsorption capacity increased as the stirring speed increased from 50 to 150 rpm. A reasonable explanation for this is that the removal efficiency increased due to the increased diffusion rate of IBP molecules from the liquid to the liquid boundary layer surrounding the Raw-RGL particles because of the turbulence formed inside the solution with a decrease in thickness of the boundary layer [60]. The sorption capacity decreased when the stirring speed was above 150 rpm due to reduced adsorbent–adsorbate interaction [61].

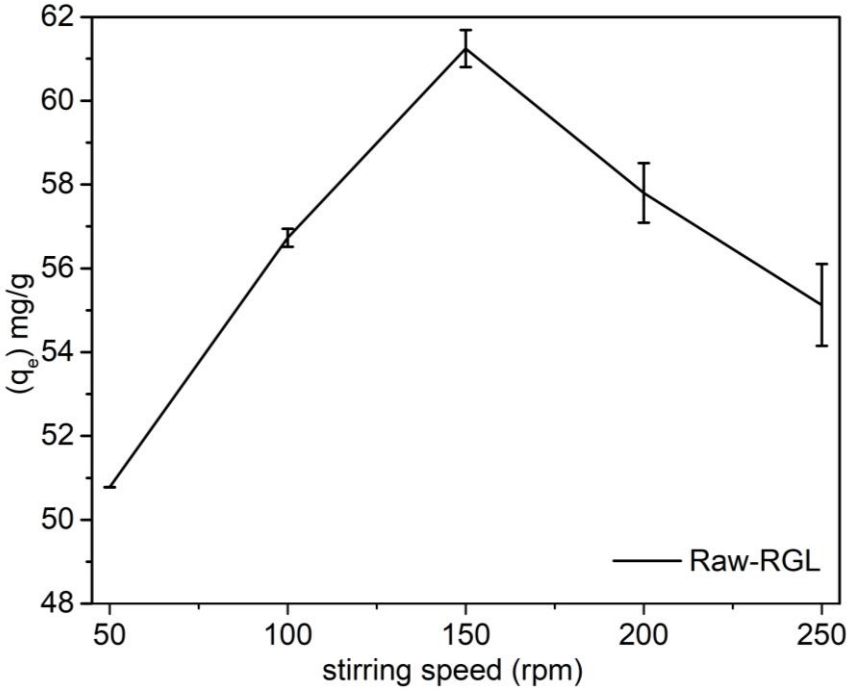

Figure 10. Effect of stirring speed on ibuprofen uptake by Raw-RGL adsorbents.

4. Regeneration Study

A reusability test of Raw-RGL and AC-RGL was conducted over four cycles (Figure 11). After each cycle, Raw-RGL and AC-RGL were regenerated before reuse. Both adsorbents lost some adsorptive capacity as the cycles continued. This is probably due to the inability of the adsorbents to desorb ibuprofen during the regeneration process. After the test, the desorbed solutions and the adsorbents were poured into separate labelled bins assigned specifically for this work. These bins are collected by a contractor or firm which specializes in disposing hazardous waste.

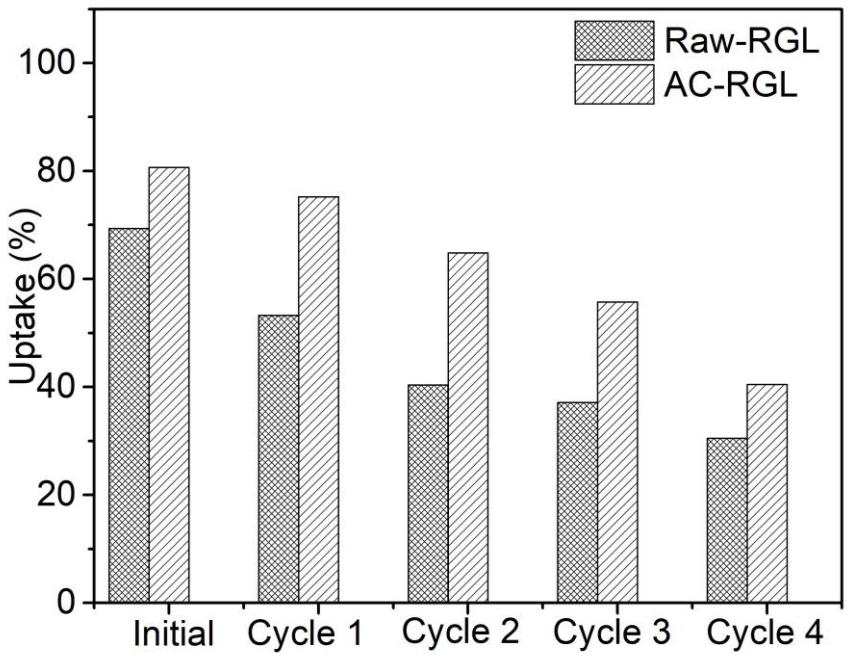

Figure 11. Reusability test of Raw-RGL and AC-RGL adsorbents.

5. Post adsorption Characterization

5.1. SEM Images

Figure 12A–D show the morphologies of the Raw-RGL and AC-RGL after the adsorption of ibuprofen. The SEM images of the Raw-RGL (Figure 12A–D) show a porous adsorbent with small cavities and longitudinal fibers. The images of AC-RGL (Figure 12C,D) show longitudinal fibers with a porous compact appearance. The longitudinal fibers are the characteristic of fibrous lignocellulosic materials [28]. As indicated in Figure 12A–D, the surface morphology of Raw-RGL and AC-RGL changed after ibuprofen adsorption. The surface morphology of both adsorbents was not so porous before adsorption but became very porous and rough after adsorption. This may be due to ibuprofen adsorption. A similar observation was made by Geng et al. (2022) [62] using plant leaves as the adsorbent. They suggested that the roughness might be attributed to the pollutants dissolving some of the organic matter in the leaves.

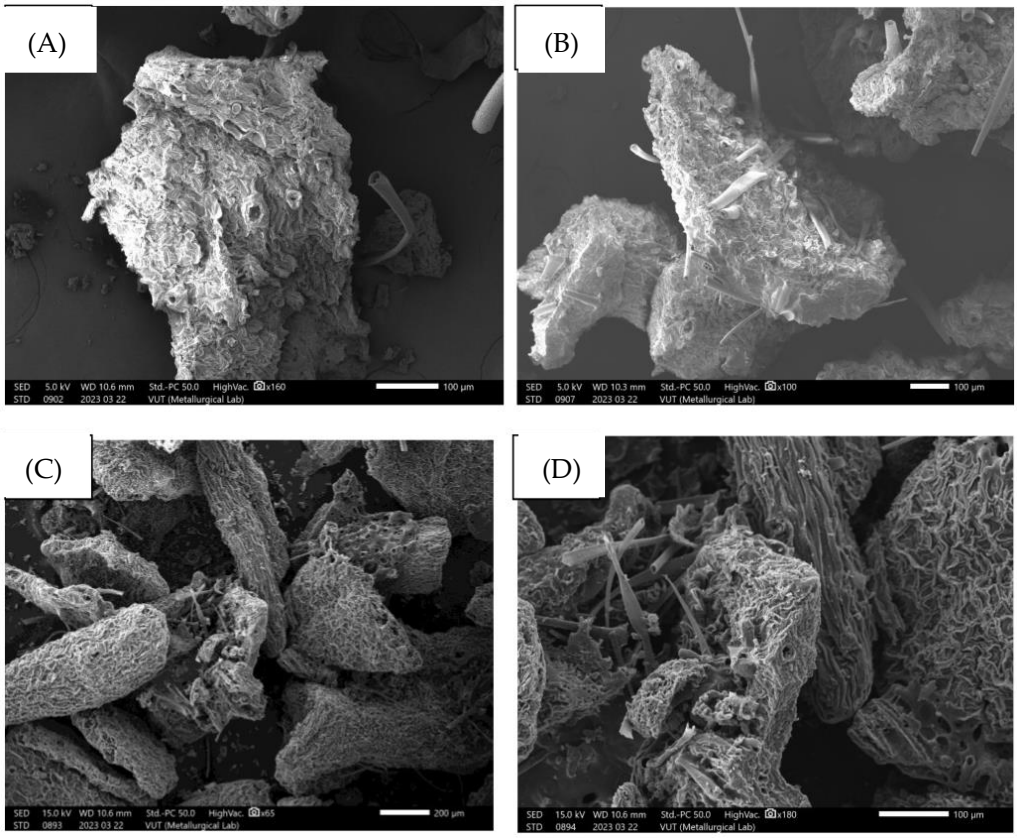

Figure 12. After adsorption, SEM images of Raw-RGL (**A**,**B**) and AC-RGL (**C**,**D**).

5.2. FTIR Analysis

The FTIR spectra of Raw-RGL and AC-RGL adsorbents after adsorption are indicated in Figure 13. The graph of Raw-RGL shows the peak at 3310 cm^{-1} due to -OH. While the -CH due to CH_2 and CH_3 shifted to 2916 and 2841 cm^{-1}, respectively. The carbonyl (-C=O) peak was clearly visible at 1724 cm^{-1} on Raw-RGL after adsorption. There were new peaks observed at 1595, 1444 and 1304 cm^{-1} after adsorption of ibuprofen on Raw-RGL. The spectrum for AC-RGL showed a peak of -C=O, which shifted to 1547 cm^{-1} after adsorption and the -O-C-O peak disappeared. The changes in wavenumbers, disappearing and formation of new peaks suggest that the functional groups were involved in the adsorption process [50].

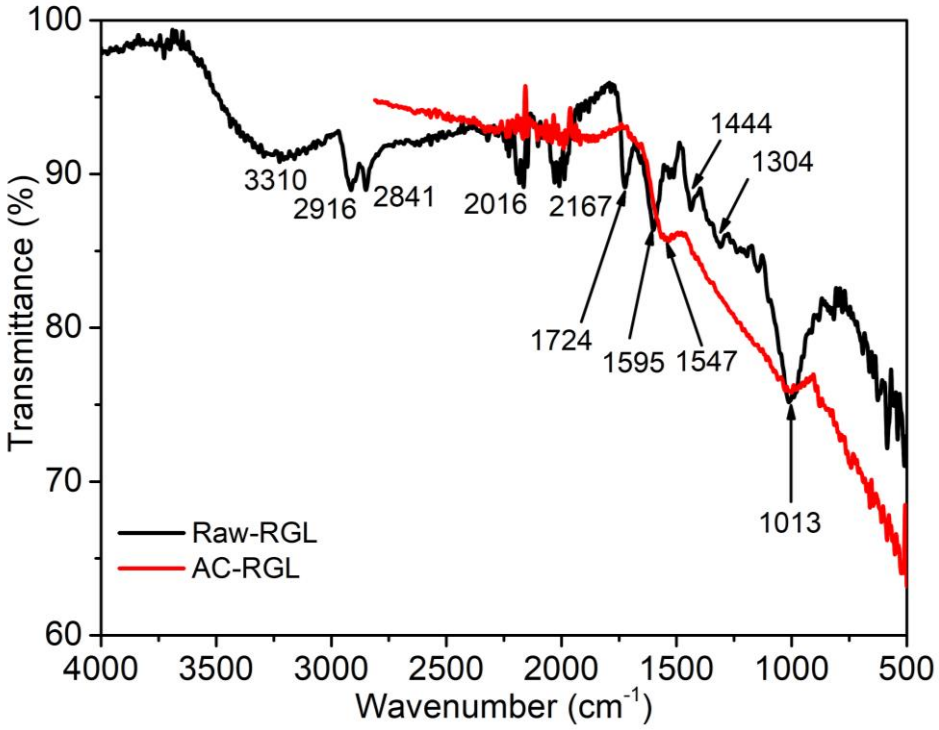

Figure 13. FTIR spectra of Raw-RGL and AC-RGL adsorbents after adsorption.

6. Comparative Studies

Table 7 shows the sorption capacities of previously reported carbon-based adsorbents for removing ibuprofen. The figures indicate the adsorption capacity of ibuprofen on Raw-RGL and AC-RGL is higher than other sorbents, suggesting that AC-RGL is a promising and cost-effective material for the uptake of ibuprofen in solution.

Table 7. Uptake of ibuprofen using activated carbon-based adsorbents.

Adsorbents	$q_{(max)}$ (mg/g)	References
	Ibuprofen	
Mesoporous carbon	120.1	[63]
Palm shell	114.7	[64]
Rose geranium leaves	113.76	This study
Standard activated carbon	85.0	[65]
Alkaline activated carbon	68.0	[66]
Yeast-based activated carbon	51.0	[67]
Leaves of mugwort weed	16.95	[68]
Sugarcane bagasse	13.51	[42]
Olive waste cake	12.9	[68]

7. Conclusions

In this study, a low-cost adsorbent was prepared from rose geranium leaves carbonized at 600 °C and chemically activated using phosphoric acid to adsorb ibuprofen in an aqueous solution. Ibuprofen sorption on activated carbon from rose geranium leaves (AC-RGL) was compared with that of natural rose geranium leaves (Raw-GRL). The sorption processes on both adsorbents were evaluated using concentration, pH effect, time and temperature. The isotherms for the Raw-RGL and AC-RGL best fitted the Freundlich model, with a correlation coefficient ranging from 0.998 to 0.997, respectively. The adsorption kinetics was ascribed to the PFO model, with a regression coefficient of 0.995 for Raw-RGL and 0.993 for AC-RGL. The thermodynamic parameter (ΔH°) for Raw-RGL and AC-RGL adsorbents indicated exothermic sorption processes. ΔS° data for ibuprofen adsorption on both adsor-

bents indicated increased randomness during adsorption. The negative figures (ΔG°) for Raw-RGL and AC-RGL adsorbents indicated that the sorption process was feasible and spontaneous. The maximum adsorption capacity and removal efficiency of AC-RGL for removing ibuprofen were 113.76 and 74.12 mg/g for Raw-RGL. These results indicate that AC-RGL is an effective and efficient adsorbent for the sorption of ibuprofen.

Author Contributions: Conceptualization, P.M.T., P.N. and F.M.; methodology, P.M.T.; formal analysis, P.M.T.; investigation, P.M.T.; resources, P.N.; data curation, P.N.; writing—original draft preparation, P.M.T.; writing—review and editing, P.N.; supervision, F.M.; project administration, P.M.T. All authors have read and agreed to the published version of the manuscript.

Funding: This research received no external funding.

Institutional Review Board Statement: Ethical clearance was obtained from the Faculty of Applied Sciences and Research Ethics Committee (FREC) of the Vaal University of Technology (VUT).

Informed Consent Statement: Informed consent was obtained from all subjects involved in the study.

Data Availability Statement: The manuscript includes all the data used in this research and its findings.

Acknowledgments: The corresponding author would like to acknowledge the support from Department of Chemistry, Vaal University of Technology, Vanderbijlpark, South Africa and collaboration from Cape Peninsula University of Technology, Cape Town, South Africa. All authours have consent to the acknowledgemnet.

Conflicts of Interest: The authors have no conflict of interest.

References

1. Oba, S.N.; Ighalo, J.O.; Aniagor, C.O.; Igwegbe, C.A. Removal of ibuprofen from aqueous media by adsorption: A comprehensive review. *Sci. Total Environ.* **2021**, *780*, 146608. [CrossRef] [PubMed]
2. Chang, E.E.; Wan, J.-C.; Kim, H.; Liang, C.-H.; Dai, Y.-D.; Chiang, P.-C. Adsorption of Selected Pharmaceutical Compounds onto Activated Carbon in Dilute Aqueous Solutions Exemplified by Acetaminophen, Diclofenac, and Sulfamethoxazole. *Sci. World J.* **2015**, *2015*, 186501. [CrossRef] [PubMed]
3. De Oliveira, M.; Atalla, A.A.; Frihling, B.E.F.; Cavalheri, P.S.; Migliolo, L.; Magalhães Filho, F.J. Ibuprofen and caffeine removal in vertical flow and free-floating macrophyte constructed wetlands with *Heliconia rostrata* and *Eichornia crassipes*. *Chem. Eng. J.* **2019**, *373*, 458–467. [CrossRef]
4. Gaffar, J.; Gabrielli, S.; Lavine, E.; Pitt, T.; Abrams, E.; Atkinson, A.; Eiwegger, T.; Protudjer, J.; Wong, T.; O'Keefe, A. Diagnosis of ibuprofen allergy through oral challenge. *Clin. Exp. Allergy* **2020**, *50*, 636–639. [CrossRef] [PubMed]
5. Davarnejad, R.; Soofi, B.; Farghadani, F.; Behfar, R. Ibuprofen removal from a medicinal effluent: A review on the various techniques for medicinal effluents treatment. *Environ. Technol. Innov.* **2018**, *11*, 308–320. [CrossRef]
6. Caicedo, D.F.; dos Reis, G.S.; Lima, E.C.; De Brum, I.A.; Thue, P.S.; Cazacliu, B.G.; Lima, D.R.; dos Santos, A.H.; Dotto, G.L. Efficient adsorbent based on construction and demolition wastes functionalized with 3-aminopropyltriethoxysilane (APTES) for the removal ciprofloxacin from hospital synthetic effluents. *J. Environ. Chem. Eng.* **2020**, *8*, 103875. [CrossRef]
7. Hanbali, G.; Jodeh, S.; Hamed, O.; Bol, R.; Khalaf, B.; Qdemat, A.; Samhan, S. Enhanced Ibuprofen Adsorption and Desorption on Synthesized Functionalized Magnetic Multiwall Carbon Nanotubes from Aqueous Solution. *Materials* **2020**, *13*, 3329. [CrossRef]
8. Streit, A.F.M.; Collazzo, G.C.; Druzian, S.P.; Verdi, R.S.; Foletto, E.L.; Oliveira, L.F.S.; Dotto, G.L. Adsorption of ibuprofen, ketoprofen, and paracetamol onto activated carbon prepared from effluent treatment plant sludge of the beverage industry. *Chemosphere* **2021**, *262*, 128322. [CrossRef]
9. Gan, Y.; Wei, Y.; Xiong, J.; Gang Cheng, G. Impact of post-processing modes of precursor on adsorption and photocatalytic capability of mesoporous TiO_2 nanocrystallite aggregates towards ciprofloxacin removal. *Chem. Eng. J.* **2018**, *349*, 1–16. [CrossRef]
10. Zhang, M.; Xiong, J.; Yang, H.; Wen, Z.; Chen, R.; Cheng, G.; Li, J.; Zhang, K.; Zhang, H. Surface potential/wettability and interface charge transfer engineering of copper-oxide (Cu-MOx, M = W, Ti, and Ce) hybrids for efficient wastewater treatment through adsorption-photocatalysis synergy. *Ind. Eng. Chem. Res.* **2020**, *59*, 15454–15463. [CrossRef]
11. Li, J.; Zhang, K.; Zhang, H. Adsorption of antibiotics on microplastics. *Environ. Poll.* **2018**, *237*, 460–467. [CrossRef] [PubMed]
12. Gan, Y.; Zhang, M.; Xiong, J.; Zhu, J.; Li, W.; Zhang, C.; Cheng, G. Impact of Cu particles on adsorption and photocatalytic capability of mesoporous Cu@TiO_2 hybrid towards ciprofloxacin antibiotic removal. *J. Taiwan Inst. Chem. Eng.* **2019**, *96*, 229–242. [CrossRef]
13. Thabede, P.M.; Shooto, N.D.; Abasi, C.; Mtunzi, F.M.; Nyamukamba, P.; Dikio, E.D. Adsorption study of lead ions on nickel-metal organic framework. *Asian J. Chem.* **2019**, *31*, 1153–1157. [CrossRef]
14. Fadzail, F.; Hasan, M.; Mokhtar, Z. Adsorption of ibuprofen using activated carbon derived from *Dillenia indica* peels. *IOP Conf. Ser. Earth Environ. Sci.* **2021**, *646*, 012031. [CrossRef]
15. Gao, Y.; Yue, Q.; Gao, B.; Sun, Y.; Wang, W.; Li, Q.; Yan, W. Preparation of high surface area-activated carbon from lignin of papermaking black liquor by KOH activation for Ni(II) adsorption. *Chem. Eng. J.* **2013**, *217*, 345–353. [CrossRef]

16. Ahmed, M.J.; Theydan, S.K. Optimization of microwave preparation conditions for activated carbon from *Albizia lebbeck* seed pods for methylene blue dye adsorption. *J. Anal. Appl. Pyrol.* **2014**, *105*, 199–208. [CrossRef]
17. Thabede, P.M.; Shooto, N.D.; Naidoo, E.B. Sorption of chromium(VI), cadmium(II) ions and methylene blue dye by pristine, defatted and carbonized *Nigella sativa* L. seeds from aqueous solution. *Asian J. Chem.* **2022**, *33*, 471–483.
18. Ofomaja, A.E. Kinetic study and sorption mechanism of methylene blue and methyl violet onto mansonia (*Mansonia altissima*) wood sawdust. *Chem. Eng. J.* **2008**, *143*, 85–95. [CrossRef]
19. Saha, P.; Chowdhury, S.; Gupta, S.; Kumar, I.; Kumar, R. Assessment on the removal of malachite green using tamarind fruit shell as biosorbent. *Clean Soil Air Water* **2010**, *38*, 437–445. [CrossRef]
20. Villabona-Ortíz, A.; Figueroa-Lopez, K.J.; Ortega-Toro, R. Kinetics and Adsorption Equilibrium in the Removal of Azo-Anionic Dyes by Modified Cellulose. *Sustainability* **2022**, *14*, 3640. [CrossRef]
21. DAFF (Department of Agriculture, Forestry and Fishery). Rose-Geranium Production. 2012. Available online: www.nda.agric.za/docs/Brochures/ProGuRosegeranium (accessed on 10 April 2022).
22. Weiss, E.A. *Essential Oil Crops*; CAB International: Wallingford, UK, 1997; pp. 125–130.
23. Motsa, N.M.; Soundy, P.; Steyn, J.M.; Learmonth, R.A.; Mojela, N.; Teubes, C. Plant shoot age and temperature effects on essential oil yield and oil composition of rose scented geranium (*Pelargonium* spp.) grown in South Africa. *J. Essent. Oil Res.* **2006**, *1*, 106–110. [CrossRef]
24. Demarne, F.E. *Geraniums and Pelargoniums: The Genera Geraniums and Pelargoniums*; Taylor and Francis: London, UK, 2002; pp. 77–93.
25. Hamidpour, R.; Hamidpour, S.; Hamidpour, M.; Marshall, V.; Hamidpour, R. Pelargonium graveolens (Rose Geranium) A Novel Therapeutic Agent for Antibacterial, Antioxidant, Antifungal and Diabetics. *Arch. Can. Res.* **2017**, *5*, 1. [CrossRef]
26. Crini, G.; Lichtfouse, E.; Chanet, G.; Morin-Crini, N. Applications of hemp in textiles, paper industry, insulation and building materials, horticulture, animal nutrition, food and beverages, nutraceuticals, cosmetics and hygiene, medicine, agrochemistry, energy production and environment. *Environ. Chem. Lett.* **2020**, *18*, 1451–1476. [CrossRef]
27. Abdel-Salam, M.A. Remediation of a Pb-Contaminated Soil Cultivated with Rose Geranium (*Pelargonium graveolens*) Using Nano-Zeolite. *J. Soil Sci. Agric. Eng. Mansoura Univ.* **2018**, *9*, 473–479. [CrossRef]
28. Beltrame, K.K.; Cazetta, A.L.; de Souza, P.S.C.; Spessato, L.; Silva, T.L.; Almeida, V.C. Adsorption of caffeine on mesoporous activated carbon fibers prepared from pineapple plant leaves. *Ecotoxicol. Environ. Saf.* **2018**, *147*, 64–71. [CrossRef] [PubMed]
29. Liu, G.; Zheng, M.; Jiang, X.; Jin, R.; Zhao, Y.; Zhan, J. Insights into the emission reductions of multiple unintentional persistent organic pollutants from industrial activities. *Chemosphere* **2016**, *144*, 420–424. [CrossRef]
30. Acosta, R.; Fierro, V.; Martinez de Yuso, A.; Nabarlatz, D.; Celzard, A. Tetracycline adsorption onto activated carbons produced by KOH activation of tyre pyrolysis charcoal. *Chemosphere* **2016**, *149*, 168–176. [CrossRef]
31. Islam, M.A.; Sabar, S.; Benhouria, A.; Khanday, W.A.; Asif, M.; Hameed, B.H. Nanoporous activated carbon prepared from karanj (*Pongamia pinnata*) fruit hulls for methylene blue adsorption. *J. Taiwan Inst. Chem. Eng.* **2017**, *74*, 96–104. [CrossRef]
32. Li, L.; Liu, S.; Zhu, T. Application of activated carbon derived from scrap tires for adsorption of Rhodamine B. *J. Environ. Sci.* **2010**, *22*, 1273–1280. [CrossRef]
33. Njoku, V.O.; Foo, K.Y.; Asif, M.; Hameed, B.H. Preparation of activated carbons from rambutan (*Nephelium lappaceum*) peel by microwave-induced KOH activation for acid yellow 17 dye adsorption. *Chem Eng. J.* **2014**, *250*, 198–204. [CrossRef]
34. Deng, H.; Li, G.; Yang, H.; Tang, J.; Tang, J. Preparation of activated carbons from cotton stalk by microwave assisted KOH and K_2CO_3 activation. *Chem. Eng. J.* **2010**, *163*, 373–381. [CrossRef]
35. Yanga, D.; Song, S.; Li, J.; Tang, Z.; Ye, J.; Yang, J. Preparation and CO_2 adsorption properties of porous carbon by hydrothermal carbonization of tree leaves. *J. Mater. Sci. Technol.* **2019**, *35*, 875–884. [CrossRef]
36. Hassana, A.F.; Elhadidy, H. Production of activated carbons from waste carpets and its application in methylene blue adsorption: Kinetic and thermodynamic studies. *J. Environ. Chem. Eng.* **2017**, *5*, 955–963. [CrossRef]
37. Boeykens, S.P.; Redondo, N.; Obeso, R.A.; Caracciolo, N.; Vázquez, C. Chromium and Lead adsorption by avocado seed biomass study through the use of Total Reflection X-Ray Fluorescence analysis. *Appl. Radiat. Isot.* **2019**, *153*, 108809. [CrossRef] [PubMed]
38. Thabede, P.M.; Shooto, N.D.; Naidoo, E.B. Removal of methylene blue dye and lead ions from aqueous solution using activated carbon from black cumin seeds. *S. Afr. J. Chem. Eng.* **2020**, *33*, 39–50. [CrossRef]
39. Danish, M.; Hashim, R.; Rafatullah, M.; Sulaiman, O.; Govind, A.A. Adsorption of Pb(II) ions from aqueous solutions by date bead carbon activated with $ZnCl_2$. *Clean Soil Air Water* **2011**, *39*, 392–399. [CrossRef]
40. Saucier, C.; Adebayo, M.A.; Lima, E.C.; Cataluna, R.; Thue, P.S.; Prola, L.D.T.; Puchana-Rosero, M.J.; Machado, F.M.; Pavan, F.A.; Dotto, G.L. Microwave-assisted activated carbon from cocoa shell as adsorbent for removal of sodium diclofenac and nimesulide from aqueous effluents. *J. Hazard. Mater.* **2015**, *289*, 18–27. [CrossRef]
41. Thabede, P.M.; Shooto, N.D.; Xaba, T.; Naidoo, E.B. Sulfuric activated carbon of black cumin (*Nigella sativa* L.) seeds for the removal of cadmium(II) and methylene blue dye. *Asian J. Chem.* **2020**, *32*, 1361–1369. [CrossRef]
42. Thabede, P.M.; Shooto, N.D.; Xaba, T.; Naidoo, E.B. Adsorption studies of toxic cadmium(II) and chromium(VI) ions from aqueous solution by activated black cumin (*Nigella sativa*) seeds. *J. Environ. Chem. Eng.* **2020**, *8*, 104045. [CrossRef]
43. Chakraborty, P.; Show, S.; Banerjee, S.; Halder, G. Mechanistic insight into sorptive elimination of ibuprofen employing bidirectional activated biochar from sugarcane bagasse: Performance evaluation and cost estimation. *J. Environ. Chem. Eng.* **2018**, *6*, 5287–5300. [CrossRef]
44. Shooto, N.D.; Thabede, P.M. Binary Adsorption of chromium and cadmium metal ions by hemp (Cannabis sativa) based adsorents. Environmental Nanotechnology. *Monit. Manag.* **2022**, *18*, 100683.

45. Daneshvar, E.; Vazirzadeh, A.; Niazi, A.; Sillanpää, M.; Bhatnagar, A. A comparative study of methylene blue biosorption using different modified brown, red and green macroalgae Effect of pre-treatment. *Chem. Eng. J.* **2017**, *307*, 435–446. [CrossRef]
46. Matos, J.; Nahas, C.; Rojas, L.; Rosales, M. Synthesis and characterization of activated carbon from sawdust of Algarroba wood. 1.Physical activation and pyrolysis. *J. Hazard. Mater.* **2011**, *196*, 360–369. [CrossRef] [PubMed]
47. Zhao, B.; Obemah David Nartey, O.D. Characterization and evaluation of biochars derived from agricultural waste biomass from Gansu, China. In Proceedings of the World Congress on Advances in Civil, Environmental, and Materials Research, Busan, Republic of Korea, 24–28 August 2014.
48. Wan, X.; Rong, Z.; Zhu, K.; Wu, Y. Chitosan-based dual network composite hydrogel for efficient adsorption of methylene blue dye. *Int. J. Biol. Macromol.* **2022**, *222*, 725–735. [CrossRef]
49. Singh, S.; Kumar, V.; Anil, A.G.; Kapoor, D.; Khasnabis, S.; Shekar, S.; Pavithra, N.; Samuel, J.; Subramanian, S.; Singh, J.; et al. Adsorption and detoxification of pharmaceutical compounds from wastewater using nanomaterials: A review on mechanism, kinetics, valorization and circular economy. *J. Environ. Manag.* **2021**, *300*, 113569. [CrossRef]
50. Mabungela, N.; Shooto, N.D.; Mtunzi, F.; Naidoo, E.B. The Adsorption of Copper, Lead Metal Ions, and Methylene Blue Dye from Aqueous Solution by Pure and Treated Fennel Seeds. *Adsorp. Sci. Technol.* **2022**, *2022*, 5787690. [CrossRef]
51. Supanchaiyamat, N.; Jetsrisupar, K.; Knijnenburg, J.T.N.; Tsang, D.C.W.; Hunt, A.J. Lignin materials for adsorption: Current trent, perspectives and opportunities. *Bioresour. Technol.* **2019**, *272*, 570–580. [CrossRef]
52. Barros, L.; Carvalho, A.M.; Ferreira, I.C.F.R. The nutritional composition of fennel (*Foeniculum vulgare*): Shoots, leaves, stems and inflorescences. *LWT-Food Sci. Technol.* **2010**, *43*, 814–818. [CrossRef]
53. Shooto, N.D.; Naidoo, E.B.; Maubane, M. Sorption studies of toxic cations on ginger root adsorbent. *J. Ind. Eng. Chem.* **2019**, *76*, 133–140. [CrossRef]
54. Sekulic, M.T.; Boskovic, N.; Slavkovic, A.; Garunovica, J.; Kolakovic, S.; Papa, S. Surface functionalised adsorbent for emerging pharmaceuticalremoval: Adsorption performance and mechanisms. *Process Saf. Environ. Prot.* **2019**, *125*, 50–63. [CrossRef]
55. Shooto, N.D.; Thabede, P.M.; Bhila, B.; Harry Moloto, H.; Naidoo, E.B. Lead ions and methylene blue dye removal from aqueous solution by mucuna beans (velvet beans) adsorbents. *J. Environ. Chem. Eng.* **2020**, *8*, 103557. [CrossRef]
56. Shooto, N.D.; Thabede, P.M.; Naidoo, E.B. Simultaneous adsorptive study of toxic metal ions in quaternary system from aqueous solution using low-cost black cumin seeds (*Nigella sativa*) adsorbents. *S. Afr. J. Chem. Eng.* **2019**, *30*, 15–27. [CrossRef]
57. Munagapati, V.S.; Dong, S.K. Adsorption of methyl orange from aqueous solution by aminated pumpkin seed powder: Kinetics, isotherms, and thermodynamic studies. *Ecotoxicol. Environ. Saf.* **2016**, *128*, 109–117.
58. Ghaedi, M.; Ansari, A.; Bahari, F.; Ghaedi, A.M.; Vafaei, A. A hybrid artificial neural network and particle swarm optimization for prediction of removal of hazardous dye brilliant green from aqueous solution using zinc sulfide. *Spectrochim. Acta A Mol. Biomol. Spectrosc.* **2015**, *137*, 1004–1015. [CrossRef] [PubMed]
59. Sarkara, S.; Tiwari, N.; Basu, A.; Behera, M.; Das, B.; Chakrabortty, S.; Sanjay, K.; Suar, M.; Adhya, T.K.; Banerjee, S.; et al. Sorptive removal of malachite green from aqueous solution by magnetite/coir pith supported sodium alginate beads: Kinetics, isotherms, thermodynamics and parametric optimization. *Environ. Technol. Innov.* **2021**, *24*, 101818. [CrossRef]
60. Basu, A.; Behera, S.S.; Dash, S.; Banerjee, S.; Sarkar, S.; Mohanty, C.K.; Dhal, N.K.; Parhi, P.K.; Tripathy, S.K. A study on removal of Cr(III) from aqueous solution using biomass of *Cymbopogon flexuosus* immobilized in sodium alginate beads and its use as hydrogenation catalyst. *J. Taiwan Inst. Chem. Eng.* **2019**, *102*, 118–132. [CrossRef]
61. Raza, M.H.; Sadiq, A.; Farooq, U.; Athar, M.; Hussain, T.; Mujahid, A.; Salman, M. Phragmites karka as a Biosorbent for the removal of mercury metal ions from aqueous solution: Effect of modification. *J. Chem.* **2015**, *2015*, 293054. [CrossRef]
62. Geng, J.; Lin, L.; Gu, F.; Chang, J. Adsorption of Cr(VI) and dyes by plant leaves: Effect of extraction by ethanol, relationship with element contents and adsorption mechanism. *Ind. Crops Prod.* **2022**, *177*, 114522. [CrossRef]
63. Jedynak, K.; Szczepanik, B.; Rędzia, N.; Słomkiewicz, P.; Kolbus, A.; Rogala, P. Ordered mesoporous carbons for adsorption of paracetamol and non-steroidal anti-inflammatory drugs: Ibuprofen and naproxen from aqueous solutions. *Water* **2019**, *11*, 1099. [CrossRef]
64. Wong, K.T.; Yoon, Y.; Jang, M. Enhanced recyclable magnetized palm shell waste based powdered activated carbon for the removal of ibuprofen: Insights for kinetics and mechanisms. *PLoS ONE* **2015**, *10*, 0141013. [CrossRef]
65. Frohlich, A.C.; dos Reis, G.S.; Pavan, F.A.; Lima, É.C.; Foletto, E.L.; Dotto, G.L. Improvement of activated carbon characteristics by sonication and its application for pharmaceutical contaminant adsorption. *Environ. Sci. Pollut. Res.* **2018**, *25*, 24713–24725. [CrossRef] [PubMed]
66. Ali, S.N.; El-Shafey, E.; Al-Busafi, S.; Al-Lawati, H.A. Adsorption of chlorpheniramine and ibuprofen on surface functionalized activated carbons from deionized water and spiked hospital wastewater. *J. Environ. Chem. Eng.* **2019**, *7*, 102860. [CrossRef]
67. Labuto, G.; Carvalho, A.P.; Mestre, A.S.; dos Santos, M.S.; Modesto, H.R.; Martins, T.D.; Lemos, S.G.; da Silva, H.G.T.; Neide, E.; Carrilho, V.M.; et al. Individual and competitive adsorption of ibuprofen and caffeine from primary sewage effluent by yeast-based activated carbon and magnetic carbon nanocomposite. *Sustain. Chem. Pharm.* **2022**, *28*, 100703. [CrossRef]
68. Dubeya, S.P.; Dwivedi, A.D.; Sillanpääa, M.; Gopal, K. *Artemisia vulgaris*-derived mesoporous honeycomb-shaped activated carbon for ibuprofen adsorption. *Chem. Eng. J.* **2010**, *165*, 537–544. [CrossRef]